Available online at www.sciencedirect.com
SCIENCE DIRECT®
Hearing Research 187 (2004) 51–62
HEARING RESEARCH
www.elsevier.com/locate/heares

Imaging of the cortical cytoskeleton of guinea pig outer hair cells using atomic force microscopy[1]

Hiroshi Wada [a,*], Kei Kimura [a], Takashi Gomi [a], Michiko Sugawara [b], Yukio Katori [c], Seiji Kakehata [d], Katsuhisa Ikeda [c], Toshimitsu Kobayashi [c]

[a] *Department of Bioengineering and Robotics, Tohoku University, Sendai 980-8579, Japan*
[b] *Department of Mechanical and Environmental Informatics, Tokyo Institute of Technology, Tokyo 152-8552, Japan*
[c] *Department of Otorhinolaryngology – Head and Neck Surgery, Tohoku University Graduate School of Medicine, Sendai 980-8574, Japan*
[d] *Department of Otorhinolaryngology, Hirosaki University School of Medicine, Hirosaki 036-8562, Japan*

Received 15 April 2003; accepted 30 September 2003

Abstract

Mammalian outer hair cells (OHCs) are known to respond to acoustical stimulation with elongation and contraction of the cells' cylindrical soma in vivo, and this motility is related to both the protein motors distributed along the OHC plasma membrane and the cytoskeleton beneath it. Therefore, the cytoskeleton seems to play an important role in the motility of the OHC. Recently, an atomic force microscope (AFM) was used to investigate the OHC cytoskeleton under physiological conditions. However, details were not made clear in that study. In this study, the ultrastructure of the cytoskeleton of fixed OHCs of guinea pigs, which were extracted with Triton X-100, was investigated using the AFM. As a result, the cortical cytoskeleton, which is formed by discrete oriented domains, was imaged, and circumferential filaments and cross-links were observed within the domain. Morphological change of the cytoskeleton of the OHC induced by diamide treatment was then examined using the AFM, and reduction of cross-links was observed. The examination indicates that the cortical cytoskeleton comprises circumferential actin filaments and spectrin cross-links.

Key words: Outer hair cell; Atomic force microscope; Cortical lattice; Actin filament; Spectrin cross-link

1. Introduction

Mammalian outer hair cells (OHCs) are known to respond to acoustical stimulation with elongation and contraction of the cells' cylindrical soma in vivo (Brownell et al., 1985; Ashmore, 1987). In vivo, the OHC is attached to the reticular lamina and a Deiters' cell only at the extreme apical surface and basal end, respectively (Kimura, 1975), and it is presumed that the force produced by the OHC, which accompanies its motility, affects the basilar membrane motion. As a result, the force production of the OHC probably leads to the fine tuning of the mammalian cochlea.

The OHC lateral wall consists of three layers: the outermost plasma membrane, the cortical lattice and the innermost subsurface cisternae. In the plasma membrane, there are protein motors which probably change their conformation according to the cell' membrane potential. As a result of their conformational change, a change in the area of the plasma membrane occurs (Adachi and Iwasa, 1999). In 2000, Zheng et al. identified the gene of the protein motor and designated it 'prestin'. In addition, Liberman et al. (2002) demonstrated that the threshold of the auditory brainstem response in prestin knockout mice is higher than that of normal mice, which shows that prestin plays an important role in the high sensitivity of hearing. The cor-

* Corresponding author: Tel.: +81 (22) 217 6938; Fax: +81 (22) 217 6939.
E-mail address: wada@cc.mech.tohoku.ac.jp (H. Wada).

[1] This study was presented at the 26th Midwinter Research Meeting of the Association for Research in Otolaryngology in February 2003.

0378-5955/03/$ – see front matter © 2003 Elsevier B.V. All rights reserved.
doi:10.1016/S0378-5955(03)00334-4

tical lattice beneath the plasma membrane is thought to convert the area change in the plasma membrane into length change in the axial direction of the cell. Therefore, the cortical lattice seems to play an important role in the motility of the OHC.

The cortical lattice consists of two types of filaments: actin and spectrin (Holley and Ashmore, 1990a; Holley et al., 1992; Nishida et al., 1993). Some electron microscopic studies utilizing transmission electron microscopy (Holley and Ashmore, 1988), the quick-freeze and deep-etching replica method (Arima et al., 1991), the freeze-etching method and negative staining (Holley et al., 1992) and the platinum replica method (Leonova and Raphael, 1999) have been performed to investigate the cytoskeleton of the OHCs. From these electron microscopic studies, it has been observed that actin filaments, which are arranged circumferentially, are 5–8 nm in diameter and are cross-linked at irregular intervals by thinner spectrins, 2–4 nm in diameter (Holley and Ashmore, 1988, 1990a,b; Arima et al., 1991; Holley et al., 1992). In the cortical lattice, protein 4.1 seems to stabilize the actin–spectrin complex (Knipper et al., 1995; Zine and Schweitzer, 1997), and the cortical lattice is connected to the plasma membrane by 'pillars' (Flock et al., 1986). The proteins that comprise the pillars remain unknown.

Although the electron microscope is a useful device for morphological research, it has some demerits in the observation of raw specimens. In principle, samples are required to be electric conductors, and a vacuum sample chamber is essential. In addition, artifacts are produced due to procedures such as fixation, dehydration, embedding, freezing, staining and replication. Alternatively, a scanning probe microscope, e.g., an atomic force microscope (AFM), can be applied to raw specimens. In this system, it is possible to image biomaterials at high resolution in liquid, and cumbersome preparations are not necessary. The AFM introduced by Binning et al. (1986) has gained some importance in the study of biological systems. It is unique because it has proven to be a suitable instrument for imaging biological samples at subnanometer resolution in their natural aqueous environment (Drake et al., 1989). The possibility of AFM application for OHCs was shown by Le Grimellec et al. (2000). Recently, Le Grimellec et al. (2002) also observed both sides of the lateral walls of OHCs of rats by tapping mode AFM, and their observations confirmed the presence of regularly aligned particles and distinguished globular and pore-like structures, the latter probably corresponding to what is expected from the OHC lateral wall motors. Wada et al. (2003) observed the lateral surface of fixed OHCs using an AFM in liquid, and circumferential filaments which were expected to be a part of the cortical lattice were shown. In addition, they reported that there was a difference between the mean spacing of circumferential filaments in the region between 0.0 and 0.85 from the basal end of the cell, i.e., in the middle and basal regions, as well as in the region between 0.85 and 1.0 from the basal end of the cell, i.e., in the apical region, and that the mean values of spacing were 54 ± 18 nm and 44 ± 17 nm, respectively. However, the detailed ultrastructure of the cortical lattice has not yet been clarified.

In this study, the ultrastructure of the cytoskeleton of the OHC was investigated in the nanoscale range under physiological conditions using an AFM. According to our experience, as living OHCs are too soft for AFM observation, OHCs must be fixed. Therefore, first, the influence of fixation and chemical treatment on cell shape changes during cell preparations was examined. AFM images on the OHC lateral wall were then acquired after the plasma membrane was removed by a detergent, Triton X-100. Finally, the morphological change of the cytoskeleton of the OHC induced by diamide treatment was examined.

2. Materials and methods

2.1. Cell isolation

Guinea pigs weighing between 200 and 300 g were used. They were decapitated and temporal bones were removed. After opening the bulla, the cochlea was detached and transferred to an experimental bath (the major ions in the medium were NaCl, 140 mM; KCl, 5 mM; $CaCl_2$, 1.5 mM; $MgCl_2 \cdot 6H_2O$, 1.5 mM; HEPES, 5 mM; glucose, 5 mM; pH 7.2; 300 mOsm). The bony shell covering the cochlea was removed and the organ of Corti was gently dissociated from the basilar membrane. The OHCs were isolated by gently pipetting the organ of Corti after enzymatic incubation with dispase (500 PU/ml). The isolated OHCs were transferred to a sample chamber and glued to MAS-coated slide glass (Matsunami glass).

The care and use of animals in this study were approved by the Institutional Animal Care and Use Committee at Tohoku University School of Medicine.

2.2. Sample preparation

First, an attempt was made to obtain AFM images of the lateral wall of OHCs without fixation. However, as the wall was very soft, it was not possible to obtain images. Therefore, the isolated OHCs were fixed with 2.5% glutaraldehyde and extracted with 2.5% Triton X-100 simultaneously in phosphate buffer (pH 7.4) for 30 min at room temperature. After fixation, the OHCs were rinsed three times with 0.1 M phosphate buffer

solution. The OHCs were then observed by the AFM in liquid.

In some experiments, diazene dicarboxylic acid bis [*N*,*N*-dimethylamide] (diamide), which reduces the actin–spectrin binding mediated by protein 4.1 in erythrocytes (Becker et al., 1986), was used for modifying the cytoskeleton of the OHC. Diamide was dissolved in the bath solutions containing dispase (250 PU/ml). The diamide concentrations were 2 or 5 mM. The dissociated organ of Corti was incubated in these solutions for 30 min at room temperature. After the incubation, the OHCs were isolated by gently pipetting the organ of Corti. Then, the isolated OHCs were transferred to a chamber and fixed and extracted in the same way as the cells which were not incubated with diamide.

2.3. Light microscopy

To investigate cell length change and local deformation due to fixation and chemical treatment, the OHCs were observed with an inverted microscope in each process of sample preparation. When local deformation was examined, the isolated OHCs were perfused with the medium, which contained microspheres 0.75 μm in diameter. With these procedures, the microspheres were randomly attached to each cell.

For examination of cell length change, the cells were observed with an inverted microscope (IX50, Olympus) and images of the cells were acquired with a CCD camera system (CS5110C, Tokyo Electronic Industry). From the acquired images, lengths of the isolated OHC before and after perfusion were analyzed.

For examination of local deformation, the cells were observed with an inverted microscope (Eclipse TE300, Nikon) and images of the cells were acquired with a CCD camera system (C2400, Hamamatsu Photonics). From these acquired images, distances between selected microspheres before and after perfusion were analyzed.

All images were analyzed off-line using a personal computer. One pixel in the recorded digital picture from the CCD camera system corresponded to 240 nm (CS5110C) and 340 nm (C2400). Each pixel was quantified using a gray scale of 256. From these images, the length of OHCs was calculated using image analysis. In addition, to analyze the position of a microsphere, a high-resolution position detection method was applied (see Wada et al., 2001). Then the distance between selected microspheres was obtained.

2.4. Atomic force microscopy

A commercial AFM (NVB100, Olympus) was used for the experiments. As the AFM unit is mounted on an inverted optical microscope, it is possible to position the tip above the cells easily. V-shaped silicon nitride cantilevers (OMCL-TR400PSA-2, Olympus) which had a pyramidal tip and a spring constant of 0.08 N/m were used. The typical radius of the curvature of the tip was less than 20 nm. In this study, as OHCs were too soft to resist lateral friction force during scanning of the contact mode due to their cylindrical shape, the oscillation imaging mode of the AFM (Tapping Mode™, Digital Instruments, Santa Barbara, CA, USA) was used. In the tapping mode AFM, the cantilever tip oscillates and touches the sample only at the end of its downward movement, which reduces the contact time and friction force as compared with the contact mode of the AFM.

In this experiment, the frequency of the cantilever tip oscillation was between 3.8 and 5.2 kHz, which is close to the resonance frequency of the cantilever tip. The scanning regions were 0.25 μm × 1.0 μm, 0.5 μm × 1.0 μm and 1.0 μm × 1.0 μm, but the scanning frequency was fixed at 0.4 Hz (scan speed: 0.4 μm/s). In all AFM images, the sample was scanned from left to right. The scanning direction corresponds to the axial direction of the OHC.

All images were analyzed by a software program by Digital Instruments (Santa Barbara, CA, USA). To correct dispersions of individual scanning lines and remove background slopes, images were plane fitted and flattened. After that, to more clearly show the fine structure in the original AFM images, their contrast was enhanced using the software program by Digital Instruments. The surface profiles were obtained by the section analysis of the original AFM images, and calculation of spacing between adjacent filaments was done by the same procedure as reported previously (Wada et al., 2003).

3. Results

3.1. Cell deformation during cell preparation

3.1.1. Change in cell length

The change in the length of the OHCs during cell preparation was measured. Fig. 1(a) shows the change in cell length when the OHCs were fixed with 2.5% glutaraldehyde and the cortical cytoskeleton was extracted with 2.5% Triton X-100 in 0.1 M phosphate buffer. The ordinate axis shows the cell length divided by the initial cell length as a percentage. From this result, the mean value of the cell length after fixation was determined to be $103.6 \pm 2.9\%$ ($n = 10$). In this report, the mean value is accompanied by standard deviation (S.D.) and the number of measurements. Fig. 1(b) shows change in cell length when the OHCs were incubated with 5 mM diamide in the experimental bath solution for 30 min. The mean value of the cell length after incubation was $100.7 \pm 3.3\%$ ($n = 16$). Fig. 1(c)

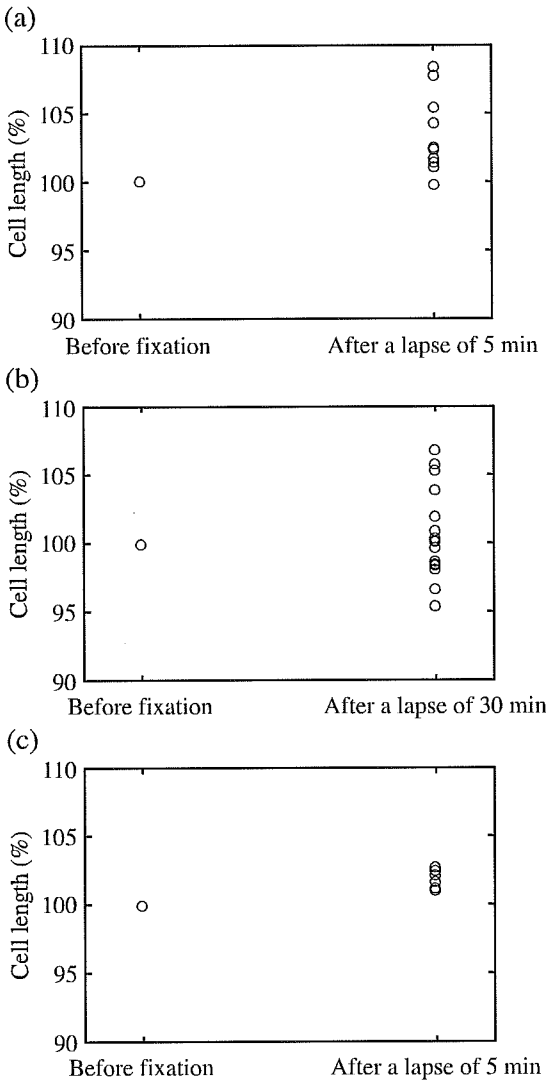

Fig. 1. Change in cell length during cell preparation. The ordinate axis shows the cell length divided by the initial cell length as a percentage. (a) OHCs were fixed with 2.5% glutaraldehyde and extracted with 2.5% Triton X-100 in 0.1 M phosphate buffer. (b) OHCs were incubated with 5 mM diamide in the experimental bath solution. (c) OHCs which had already been incubated with 5 mM diamide were fixed with 2.5% glutaraldehyde and extracted with 2.5% Triton X-100 in 0.1 M phosphate buffer.

shows the change in cell length when the OHCs were fixed with 2.5% glutaraldehyde and extracted with 2.5% Triton X-100 in 0.1 M phosphate buffer after incubation with 5 mM diamide for 30 min. The mean value of the cell length after fixation was $101.8 \pm 0.7\%$ ($n = 7$).

3.1.2. Local deformation

Local deformation of the OHC during cell preparation was measured. Fig. 2a–c shows local deformation of the OHC under the same chemical conditions as shown in Fig. 1(a–c), respectively. Fig. 2(a) presents an example of the measurement points on the cell and the rate of local deformation when the OHCs were fixed with 2.5% glutaraldehyde and extracted with 2.5% Triton X-100 in 0.1 M phosphate buffer. After a lapse of 5 min, the distances between selected microspheres, 1–2, 2–3 and 1–3, were 104.4%, 103.6% and 103.7%, respectively. A total of three cells were examined and local deformations changed from 98.2% to 104.4%. Fig. 2(b) shows an example of the rate of local deformation when the OHCs were incubated with 5 mM diamide in the experimental bath solution for 30 min. After a lapse of 30 min, the distances between selected microspheres, 1–2, 2–3 and 1–3, were 99.5%, 97.8% and 98.6%, respectively. A total of three cells were examined and local deformations changed from 97.8% to 105.5%. Fig. 2(c) presents an example of the rate of local deformation when the OHCs were fixed with 2.5% glutaraldehyde and extracted with 2.5% Triton X-100 in 0.1 M phosphate buffer after incubation with 5 mM diamide for 30 min. The distances between selected microspheres, 1–2, 2–3 and 1–3, were 101.8%, 101.6% and 102.2%, respectively. A total of four cells were examined and local deformations changed from 101.4% to 103.7%. In all conditions, the rate of local deformations tended to agree with the rate of change in cell length, and distortions, i.e., differences in local deformations were not observed.

3.2. Morphology of the cytoskeleton of the OHC

The cytoskeleton of the lateral wall of the fixed OHC which was extracted with Triton X-100 was imaged with tapping mode AFM. Fig. 3(a) depicts the measured rectangular region. Fig. 3(b) shows an original AFM image of the cortical cytoskeleton acquired in that region and Fig. 3(c) shows the AFM image which was obtained by enhancing the contrast of Fig. 3(b). In AFM images, the brighter regions correspond to higher ones of the sample surfaces, and the transverse direction in the AFM images corresponds to the axial direction of the OHC. In the AFM images, a cytoskeletal lattice is seen to be formed by some differently oriented domains. Within each domain, relatively thick circumferential filaments run approximately parallel to each other, and they are cross-linked regularly or irregularly by thinner filaments. A schematic of the domains and filaments shown in Fig. 3(c) is displayed in Fig. 3(d). In this figure, the schematic only shows clearly recognized areas. The boundary of the domains, the circumferential filaments and the cross-links are shown by dotted lines, thick solid lines and thin solid lines, respectively. Such lattices, composed of these discrete domains and two types of filaments, were observed along the full length of the OHC lateral wall. Fig. 4 shows another

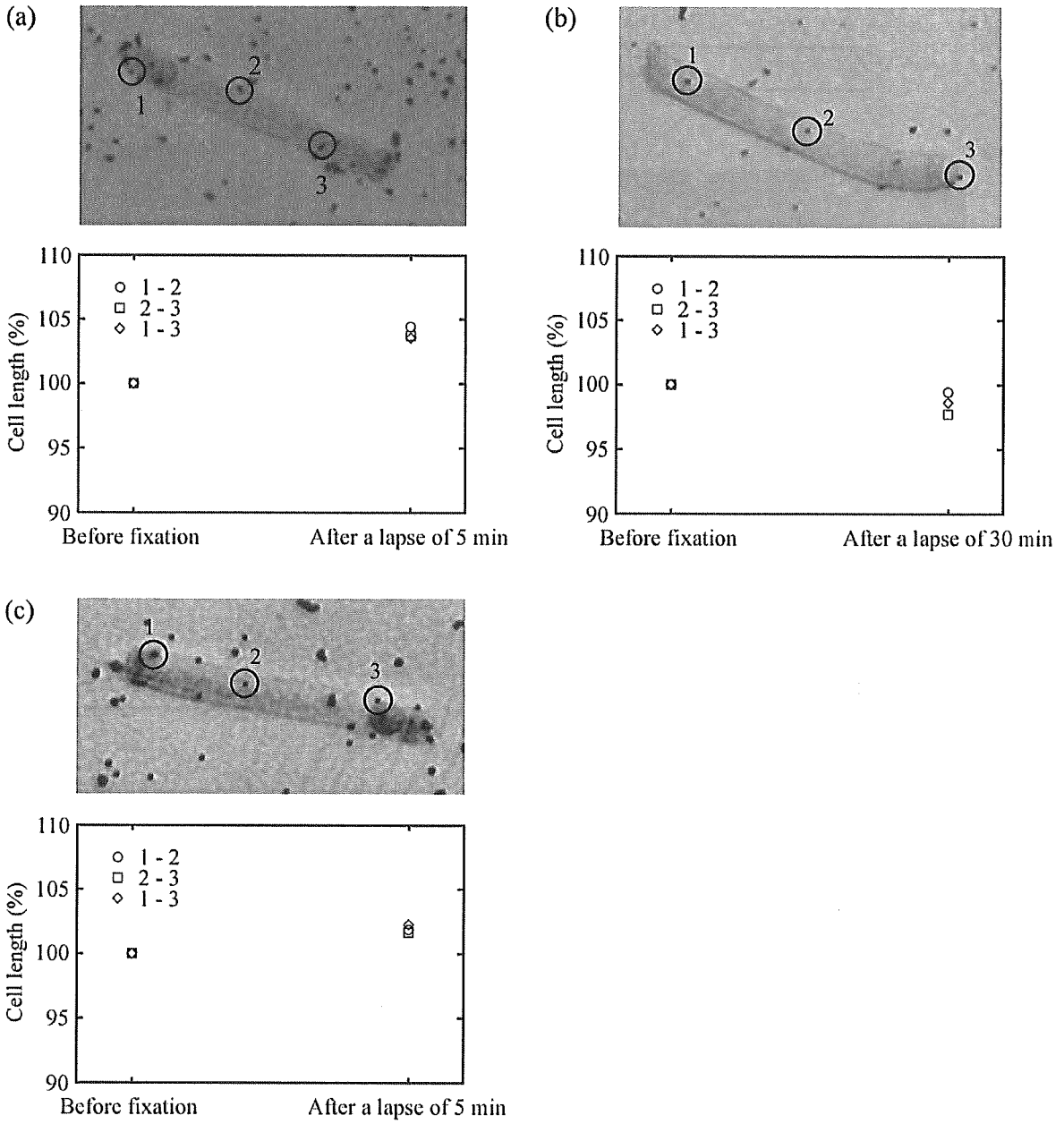

Fig. 2. Local deformation of the OHC during cell preparation. Black points are microspheres and those marked by the open circles are measurement points. The ordinate axis shows the cell length divided by the initial cell length as a percentage. (a) OHCs were fixed with 2.5% glutaraldehyde and extracted with 2.5% Triton X-100 in 0.1 M phosphate buffer. (b) OHCs were incubated with 5 mM diamide in the experimental bath solution. (c) OHCs which had already been incubated with 5 mM diamide were fixed with 2.5% glutaraldehyde and extracted with 2.5% Triton X-100 in 0.1 M phosphate buffer. 1–2, 1–3 and 2–3 represent the distances between the respective numbered microspheres.

AFM image of the cortical lattice obtained in the basal region. Circumferential filaments and cross-links are seen here as well. However, differently oriented domains shown in Fig. 3(c) are not observed in this image.

3.3. Spacing of circumferential filaments

In this study, spacing between circumferential filaments within a domain was evaluated in the region between 0.0 and 0.85 from the basal end of the cell, i.e., in the middle and basal regions, and in the region between 0.85 and 1.0 from the basal end of the cell, i.e., in the apical region. The mean spacing, S.D., number of measurements and number of cells in each region are shown in Table 1. The mean spacing ± S.D. of circumferential filaments in the middle and basal regions was

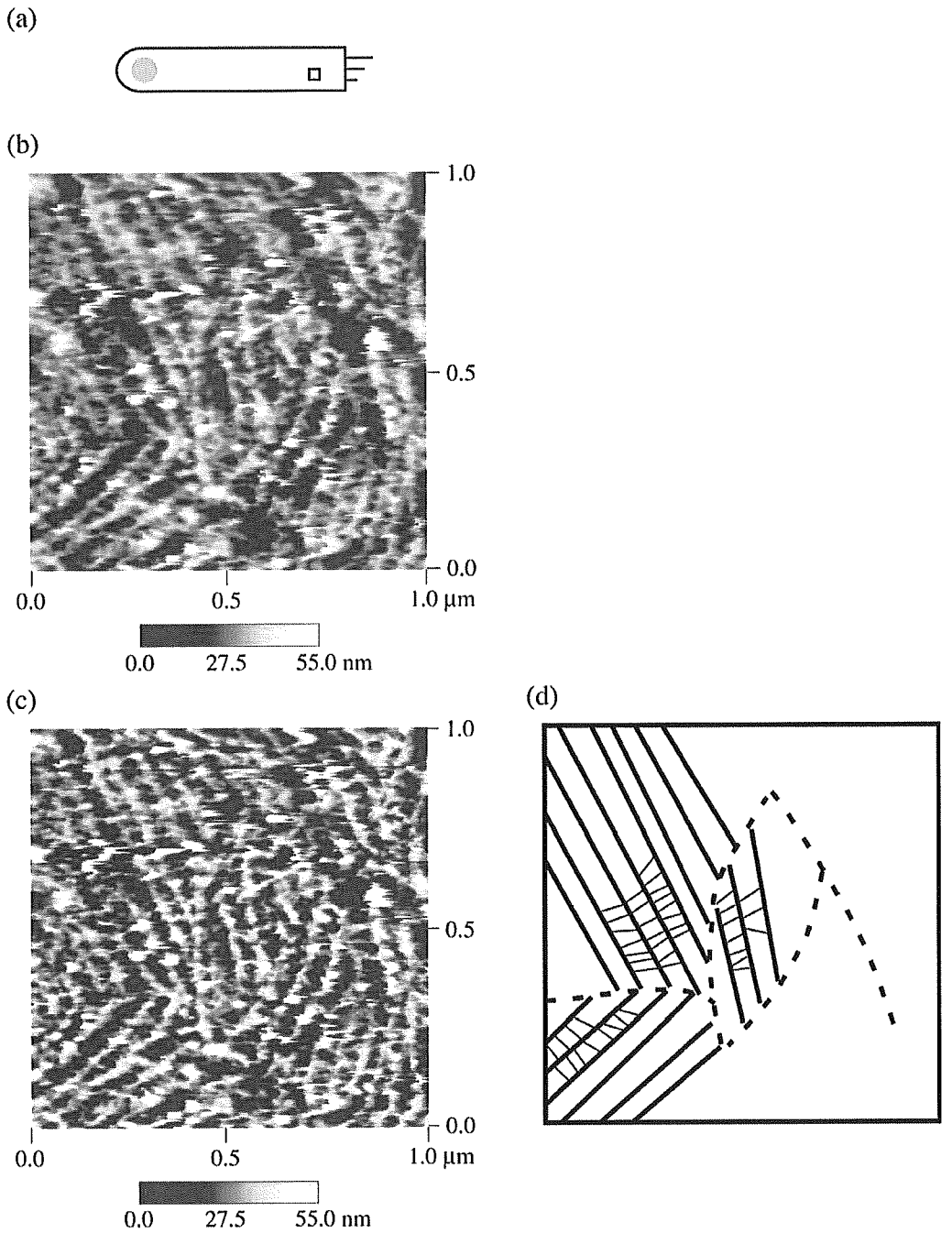

Fig. 3. An AFM image of the cytoskeleton in the OHC lateral wall. The OHC was fixed by 2.5% glutaraldehyde and demembraned with 2.5% Triton X-100. (a) The position of the scanning area. (b) The original AFM image acquired in the rectangular region in panel a. The scanning area and frequency were 1.0 μm × 1.0 μm and 0.4 Hz, respectively. The lattice is formed by some differently oriented domains. Within each domain, thicker circumferential filaments are cross-linked by thinner filaments. (c) The contrast-enhanced image of panel b. (d) A schematic of the domains and filaments in panel c. In this figure, the schematic only shows clearly recognized areas. Boundary lines of domains, circumferential filaments and cross-links are shown by dotted lines, thick solid lines and thin solid lines, respectively.

51.5 ± 9.78 nm ($n = 550$), whereas that in the apical region was 47.0 ± 10.2 nm ($n = 352$). As the number of measurements was in the hundreds, it was appropriate to apply the parametric method for statistical evaluation. The difference between the mean spacing in the middle and basal regions and that in the apical region was statistically significant at $P < 0.0001$ using Student's t-test.

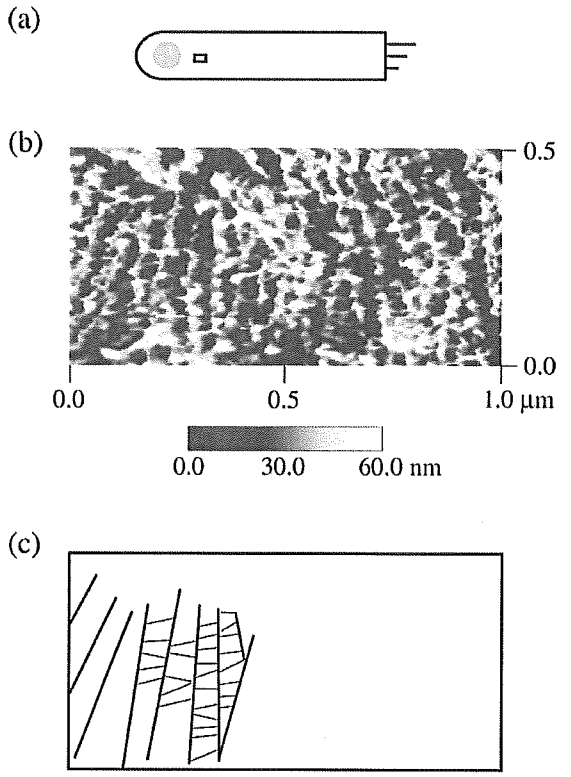

Fig. 4. A contrast-enhanced AFM image of the cytoskeleton in the OHC lateral wall. The OHC was fixed by 2.5% glutaraldehyde and demembraned with 2.5% Triton X-100. (a) The position of the scanning area. (b) The AFM image acquired in the rectangular region in panel a. The scanning area and frequency were 0.5 μm×1.0 μm and 0.4 Hz, respectively. Thicker circumferential filaments are cross-linked by thinner filaments. Differently oriented domains are not seen in this image. (c) A schematic of the two types of filaments in panel b. The schematic only shows clearly recognized areas. Circumferential filaments and cross-links are shown by thick and thin solid lines, respectively.

3.4. Spacing of cross-links

In the same way as mentioned in Section 3.3, the OHC was divided into the middle and basal regions and the apical region, and the spacing of cross-links in each region was evaluated. From the AFM images shown in Figs. 3(c) and 4(b), it can be seen that cross-links are not arranged parallel to each other and that they appear as branched links in some places. Therefore, when the spacing of cross-links was evaluated in this study, as shown in Fig. 5, the mean distance between the adjacent cross-links at both ends was determined to be the spacing of adjacent cross-links, and branched links were ignored. The mean spacing, S.D., number of measurements and number of cells in individual regions are shown in Table 2. The mean spacing ± S.D. of the cross-links in the middle and basal regions was 24.9 ± 6.85 ($n = 214$), and that in the apical region was 25.7 ± 7.29 ($n = 86$). In contrast to the spacing of the circumferential filaments, there was no statistically significant difference between the mean spacing in the apical region and that in the middle and basal regions.

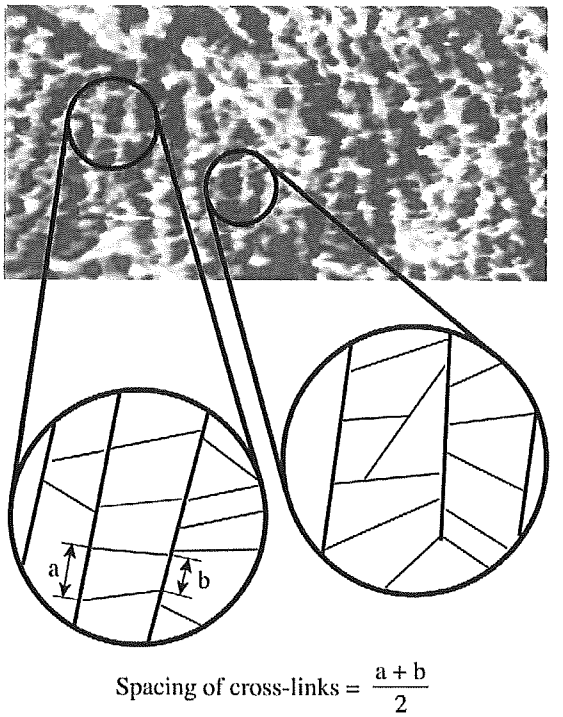

Fig. 5. Measurement of the spacing of adjacent cross-links. The mean distance between the adjacent cross-links at both ends was determined to be the spacing of the cross-links (see the left circle); branched links (see the right circle) were ignored.

3.5. Effect of diamide on the structure of the OHC cytoskeleton

Some OHCs were incubated with diamide, which is a sulfhydryl-oxidizing agent. The cytoskeleton of diamide-treated OHCs which were fixed with 2.5% glutaraldehyde and extracted with 2.5% Triton X-100 was imaged using the tapping mode AFM. Fig. 6 shows

Table 1
Spacing of the circumferential filaments in the middle and basal regions and that in the apical region

Region	Mean (nm)	S.D. (nm)	Number of measurements	Number of cells
Middle and basal regions	51.5	9.78	550	15
Apical region	47.0	10.2	352	13

Difference between means in these two regions was statistically significant at $P < 0.0001$ using Student's t-test.

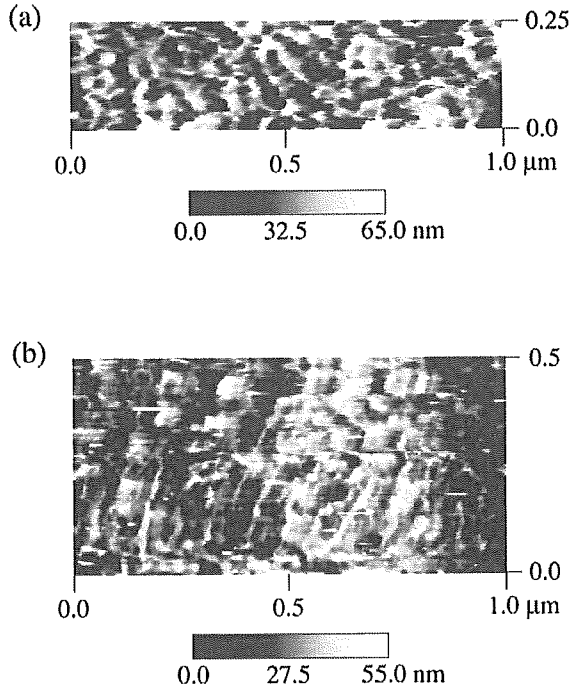

Fig. 6. Contrast-enhanced AFM images of the diamide treated cytoskeleton in the OHC lateral wall. The OHC was fixed by 2.5% glutaraldehyde and demembraned with 2.5% Triton X-100 after incubation with 2 or 5 mM diamide. (a) The OHC was incubated with 2 mM diamide. The scanning area and frequency were 0.25 μm×1.0 μm and 0.4 Hz, respectively. Circumferential filaments are recognized, and cross-links are observed in many areas. (b) The OHC was incubated with 5 mM diamide. The scanning area and frequency were 0.5 μm×1.0 μm and 0.4 Hz, respectively. Many circumferential filaments are recognized; however, cross-links are hardly seen.

AFM images of the cortical lattice modified by 2 and 5 mM diamide. In Fig. 6a, circumferential filaments are seen and cross-links are observed in many areas. However, in Fig. 6b, although many circumferential filaments are recognized, cross-links are hardly seen. Comparing Fig. 4 with Fig. 6, structural change in the cytoskeleton due to the diamide incubation is clear. Diamide treatment reduced cross-links in AFM images. The spacing of circumferential filaments was evaluated in diamide-treated OHCs. Fig. 7 shows the relationship between the concentration of diamide and the mean spacing of circumferential filaments in the middle and basal regions. From this figure, it is clear that the spacing of circumferential filaments decreased with an increase in the concentration of diamide. The difference

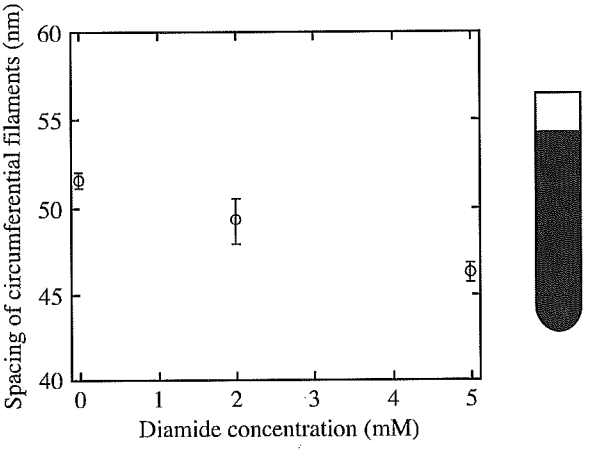

Fig. 7. Relationship between the diamide concentration and the spacing of circumferential filaments in the middle and basal regions of the OHC. Bars indicate standard errors. OHCs were incubated in the media which contained diamide for 30 min at room temperature. Diamide treatment induced the reduction of the spacing of circumferential filaments. The difference between the mean spacing of cells which were not incubated with diamide and that of cells incubated with 5 mM diamide is statistically significant at $P<0.0001$ using Student's t-test.

between the mean spacing of cells which were not incubated with diamide and that of cells incubated with 5 mM diamide was statistically significant at $P<0.0001$ using Student's t-test. In contrast to the middle and basal regions, as shown in Fig. 8, the mean spacing was not related to diamide concentration in the apical region. The difference between the mean spacing of cells which were not incubated with diamide and that of cells incubated with 5 mM diamide was not statistically significant.

4. Discussion

4.1. Influence of cell preparation

Tapping mode AFM in liquid was used for the morphological study of the OHC cytoskeleton. This method allowed a visualization of the OHC lateral wall under physiological conditions. However, as the living OHCs were too soft for AFM observation, the OHCs had to be fixed by glutaraldehyde. Slepecky and Ulfendahl (1988) reported that glutaraldehyde induced shortening of OHCs and that length changes up to 10% of the total

Table 2
Spacing of the cross-links in the middle and basal regions and that in the apical region

Region	Mean (nm)	S.D. (nm)	Number of measurements	Number of cells
Middle and basal regions	24.9	6.85	214	4
Apical region	25.7	7.29	86	3

Difference between means in these two regions was not statistically significant.

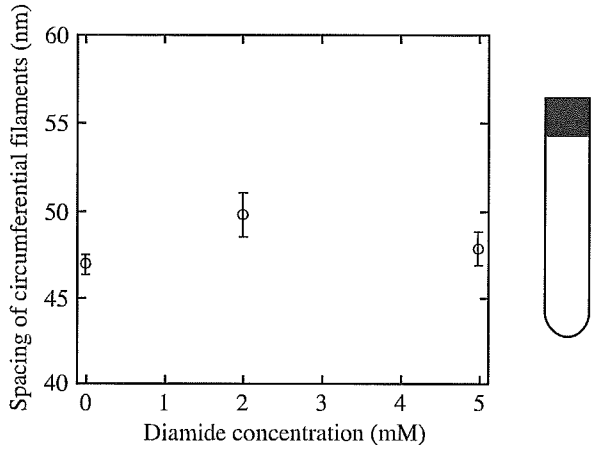

Fig. 8. Relationship between the diamide concentration and the spacing of circumferential filaments in the apical region of the OHC. Bars indicate standard errors. There is no significant relationship between the diamide concentration and the spacing of circumferential filaments. The difference between the mean spacing of cells which were not incubated with diamide and that of cells incubated with 5 mM diamide is not statistically significant.

cell length were observed over a period of 5 min. On the other hand, Holley et al. (1992) reported that when the effects of glutaraldehyde fixation on the extracted lattice were observed by light microscope, cell shape changes were not detected. In this study, when the effect of glutaraldehyde fixation and Triton X-100 extraction on whole cell length of OHCs was observed by the optical inverted microscope, the OHCs were found to be extended only $3.6 \pm 2.9\%$ ($n = 10$) and distortion of local deformations, i.e., the difference in local deformations, was not observed after a lapse of 5 min. Therefore, it is estimated that the OHCs were fixed without deformation macroscopically and that the OHCs retained the same morphology as when they were under physiological conditions. In some experiments, the OHCs were fixed with 2.5% glutaraldehyde and extracted with 2.5% Triton X-100 in 0.1 M phosphate buffer after incubation with 2 and 5 mM diamide in the experimental bath solution for 30 min. Through these sequential preparations, the OHCs were extended by only a few percentage points and distortion was not observed.

4.2. Structure of the cortical lattice in AFM images

In many images, as shown in Fig. 3, the cortical lattice is formed by differently oriented domains, and within a domain, thick circumferentially filaments and thin cross-links form lattice structures. Cross-links of the cortical cytoskeleton of the OHC were visualized by AFM for the first time. The cross-links are not arranged parallel to each other and appear as branched links, though the circumferential filaments are arranged approximately parallel to each other within a domain. In this study, pillars were not preserved, presumably due to the permeabilization of Triton X-100.

Diamide is a specific oxidizing reagent for the sulfhydryl group (Kosower and Kosower, 1995). In erythrocytes, diamide increases intermolecular links between spectrin molecules (Haest et al., 1977; Maeda et al., 1983) and reduces the actin–spectrin binding mediated by protein 4.1 (Becker et al., 1986). The reduction of cross-links in the AFM image in this study, observed on

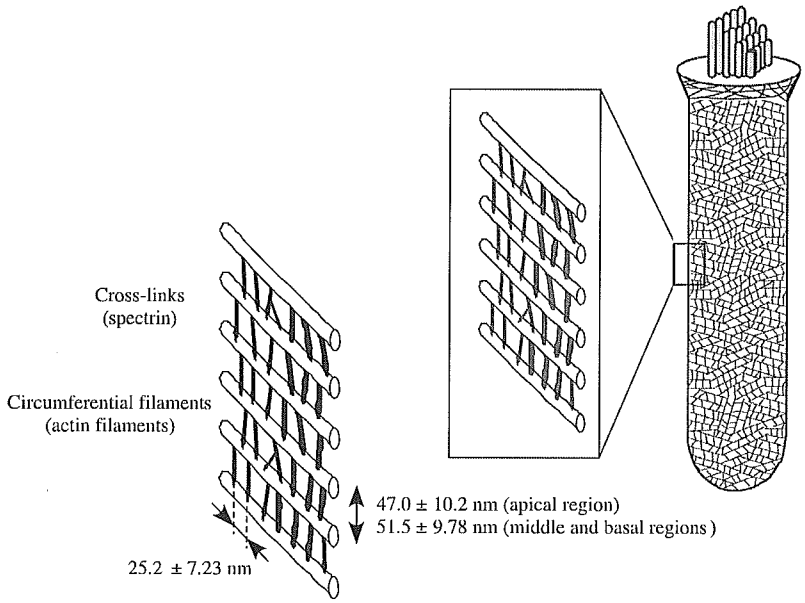

Fig. 9. A scheme of the cortical lattice. The cortical lattice is formed by differently oriented domains; such domains consist of circumferential filaments, which are composed of actin, arranged approximately parallel to each other and cross-links, which are composed of spectrin, connected to adjacent actin filaments.

the lateral wall of the diamide treated OHC, would be due to the fact that the diamide treatment reduces the actin–spectrin binding mediated by protein 4.1. From immunological evidence, it is known that the cortical lattice is composed of actin and spectrin (Flock et al., 1986; Nishida et al., 1993). Therefore, it is suggested that the circumferential filaments are actin filaments and that the cross-links are spectrin. This idea is supported by the fact that the diamide treatment reduces the axial stiffness of the OHC in a dose-dependent manner (Adachi and Iwasa, 1997), which makes the cell highly extendable in axial direction (Frolenkov et al., 1998).

A scheme of the OHC cortical lattice is shown in Fig. 9. The cortical lattice is formed by differently oriented domains; such domains consist of circumferential filaments, which are composed of actin, arranged approximately parallel to each other and cross-links, which are composed of spectrin, connected to adjacent actin filaments.

4.3. Comparison between results of this experiment and those of previous studies

Features of the cortical lattice mentioned in Section 4.2 agree with previous findings (Holley and Ashmore, 1990a,b; Arima et al., 1991; Holley et al., 1992). From electron microscopic studies, it has been reported that the spacing of circumferential filaments is from 30 to 80 nm and that that of cross-links is from 10 to 50 nm. In this experiment, the mean spacing ± S.D. of circumferential filaments and that of cross-links are 51.5 ± 9.78 and 24.9 ± 6.85 nm, respectively (middle and basal regions), and these values correspond to the values obtained from electron microscopic images.

In our previous study (Wada et al., 2003), we observed the lateral surface of the fixed OHC by tapping mode AFM in liquid without Triton X-100 extraction. As a result, not discrete domains and cross-links but circumferentially arranged filaments were observed. We reported that there was a difference between the mean spacing of circumferential filaments in the middle and basal regions and that in the apical region, and speculated that the circumferential filaments were a part of the cortical lattice. Le Grimellec et al. (2002) observed the lateral surface of fixed OHCs (0.8% glutaraldehyde) of rats by tapping mode AFM. They demonstrated that increasing the tapping force led to the reversible visualization of circumferential stripes and that the mean distance between stripes was 41 ± 3 nm. According to their explanation, the stripes are likely a part of the cytoskeleton of the OHC lateral wall.

In this study, differently oriented domains, relatively thick circumferential filaments and thinner cross-links were recognized in AFM images of the OHC lateral wall extracted with Triton X-100. The mean spacing of circumferential filaments is close to the value reported by Wada et al. (2003) and there is also a difference between the mean spacing of circumferential filaments in the middle and basal regions and that in the apical region. Therefore, it is estimated that the circumferential filaments in the AFM images of this investigation correspond to those reported by Wada et al. (2003). In this study, discrete domains of circumferential filaments, not shown by Wada et al. (2003), were observed in the AFM images. The reason for the discrepancy between the two observations is that the cytoskeleton of the OHC lateral wall was visualized directly in this experiment, whereas Wada et al. (2003) observed the cytoskeleton indirectly via the plasma membrane.

4.4. Apical region and the other regions

There is a difference between the mean spacing of circumferential filaments in the middle and basal regions and that in the apical region. The same finding has also been previously reported (Wada et al., 2003). It is expected that the difference in the mean spacing is one factor that causes the high stiffness in the apical region of the OHC (Wada et al., 2001). As the cross-links hold the cell shape in the axial direction, it is expected that the contribution of cross-links to the axial stiffness of the OHC is greater than that of the circumferential filaments. However, there is no significant difference between the mean spacing of cross-links in the middle and basal regions and that in the apical region in spite of the high axial stiffness in the apical region of the OHC. Therefore, it is expected that spectrin cross-links do not contribute to the non-uniformity of the local stiffness of the OHC.

When the OHCs were incubated with diamide, although the cell length did not change, the mean spacing of circumferential filaments microscopically decreased in a dose-dependent fashion without macroscopical distortions in the middle and basal regions, whereas the mean spacing of circumferential filaments did not decrease in the apical region. One possible reason might be that the domains change their orientation when spectrin cross-links decrease and that this change results in adjustment of cell length. On the other hand, the unaltered mean spacing of circumferential filaments in the apical region might have its origin in the intracellular organelle under the cortical lattice. Saito (1983) reported that the endoplasmic reticulum, Golgi apparatus, lamellar bodies, multivesicular bodies and dilated cisterns are located in the apical cytoplasm beneath the cuticular plate. The presence of actin filaments (Lim and Melnick, 1971) and microtubules (Raphael and Wroblewski, 1986) under the subsurface cisternae has

been previously reported. Also, Leonova and Raphael (1999) reported the presence of a thin, dense layer of actin filaments under the subsurface cisternae. Therefore, it is estimated that the cortical lattice interacts with intracellular organelles via the subsurface cisternae and the dense layer of actin filaments and microtubules under the subsurface cisternae in the apical region of the OHC. As a result, the spacing of circumferential filaments in the apical region of diamide-treated OHCs does not change in the absence of spectrin cross-links.

5. Conclusions

The ultrastructure of the exposed cytoskeleton of the fixed OHC lateral wall was observed by AFM under physiological conditions, and the following conclusions were drawn:

1. The cortical lattice comprises many domains, which are composed of circumferential filaments and cross-links.
2. It was confirmed by diamide treatment that circumferential filaments and cross-links are actin filaments and spectrins, respectively.
3. The mean spacing ± S.D. of circumferential actin filaments in the middle and basal regions and that in the apical region were determined to be 51.5 ± 9.78 and 47.0 ± 10.2 nm, respectively.
4. The mean spacing ± S.D. of spectrin cross-links was found to be 25.2 ± 7.23 nm.
5. Due to diamide treatment, the mean spacing of circumferential actin filaments decreases in a dose-dependent fashion in the middle and basal regions of the OHC, although the length of the cell is constant.

Acknowledgements

This work was supported by a grant from the Human Frontier Science Program, by a Health and Labour Science Research Grant from the Ministry of Health, Labour and Welfare of Japan, by a Grant-in-Aid for Scientific Research (A) 11307033, and a Grant-in-Aid for Scientific Research on Priority Areas 15086202 from the Ministry of Education, Science, Sports and Culture of Japan.

References

Adachi, M., Iwasa, K.H., 1997. Effect of diamide on force generation and axial stiffness of the cochlear outer hair cell. Biophys. J. 73, 2809–2818.

Adachi, M., Iwasa, K.H., 1999. Electrically driven motor in the outer hair cell: Effect of a mechanical constraint. Proc. Natl. Acad. Sci. USA 96, 7244–7249.

Arima, T., Kuraoka, A., Toriya, R., Shibata, Y., Uemura, T., 1991. Quick-freeze, deep-etch visualization of the 'cytoskeletal spring' of cochlear outer hair cells. Cell Tissue Res. 263, 91–97.

Ashmore, J.F., 1987. A fast motile response in guinea-pig outer hair cells: the cellular basis of the cochlear amplifier. J. Physiol. 388, 323–347.

Becker, P.S., Cohen, C.M., Lux, S.E., 1986. The effect of mild diamide oxidation on the structure and function of human erythrocyte spectrin. J. Biol. Chem. 261, 4620–4628.

Binning, G., Quate, C.F., Gerber, Ch., 1986. Atomic force microscope. Phys. Rev. Lett. 56, 930–933.

Brownell, W.E., Bader, C.R., Bertrand, D., de Ribaupierre, Y., 1985. Evoked mechanical responses of isolated cochlear outer hair cells. Science 227, 194–196.

Drake, B., Prater, C.B., Weisenhorn, A.L., Gould, S.A.C., Albrecht, T.R., Quate, C.F., Cannell, D.S., Hansma, H.G., Hansma, P.K., 1989. Imaging crystals, polymers, and processes in water with the atomic force microscope. Science 243, 1586–1588.

Flock, A., Flock, B., Ulfendahl, M., 1986. Mechanisms of movement in outer hair cells and a possible structural basis. Arch. Otorhinolaryngol. 243, 83–90.

Frolenkov, G.I., Atzori, M., Kalinec, F., Mammano, F., Kachar, B., 1998. The membrane-based mechanism of cell motility in cochlear outer hair cells. Mol. Biol. Cell 9, 1961–1968.

Haest, C.W., Kamp, D., Plasa, G., Deuticke, B., 1977. Intra- and intermolecular cross-linking of membrane proteins in intact erythrocytes and ghosts by SH-oxidizing agents. Biochim. Biophys. Acta 469, 226–230.

Holley, M.C., Ashmore, J.F., 1988. A cytoskeletal spring in cochlear outer hair cells. Nature 335, 635–637.

Holley, M.C., Ashmore, J.F., 1990a. Spectrin, actin and the structure of the cortical lattice in mammalian cochlear outer hair cells. J. Cell Sci. 96, 283–291.

Holley, M.C., Ashmore, J.F., 1990b. A cytoskeletal spring for the control of cell shape in outer hair cells isolated from the guinea pig cochlea. Eur. Arch. Oto-Rhino-Laryngol. 247, 4–7.

Holley, M.C., Kalinec, F., Kachar, B., 1992. Structure of the cortical cytoskeleton in mammalian outer hair cells. J. Cell Sci. 102, 569–580.

Kimura, R.S., 1975. The ultrastructure of the organ of Corti. Int. Rev. Cytol. 42, 173–222.

Knipper, M., Zimmermann, U., Köpschall, I., Rohbock, K., Jüngling, S., Zenner, H.P., 1995. Immunological identification of candidate proteins involved in regulating active shape changes of outer hair cells. Hear. Res. 86, 100–110.

Kosower, N.S., Kosower, E.M., 1995. Diamide: an oxidant probe for thiols. Methods Enzymol. 251, 123–133.

Le Grimellec, C., Giocondi, M-C., Pujol, R., Lesniewska, E., 2000. Tapping mode atomic force microscopy allows the in situ imaging of fragile membrane structures and of intact cells surface at high resolution. Single Mol. 1, 105–107.

Le Grimellec, C., Giocondi, M-C., Lenoir, M., Vater, M., Sposito, G., Pujol, R., 2002. High-resolution three-dimensional imaging of the lateral plasma membrane of cochlear outer hair cells by atomic force microscopy. J. Comp. Neurol. 451, 62–69.

Leonova, E.V., Raphael, Y., 1999. Application of platinum replica method to the study of the cytoskeleton of isolated hair cells, supporting cells and whole mounts of the organ of Corti. Hear. Res. 130, 137–154.

Liberman, M.C., Gao, J., He, D.Z.Z., Wu, X., Jia, S., Zuo, J., 2002. Prestin is required for electromotility of the outer hair cell and for the cochlear amplifier. Nature 419, 300–304.

Lim, D.J., Melnick, W., 1971. Acoustic damage of the cochlea. A

scanning and transmission electron microscopic observation. Arch. Otolaryngol. 94, 294–305.

Maeda, N., Kon, K., Imaizumi, K., Sekiya, M., Shiga, T., 1983. Alteration of rheological properties of human erythrocytes by crosslinking of membrane proteins. Biochim. Biophys. Acta 735, 104–112.

Nishida, Y., Fujimoto, T., Takagi, A., Honjo, I., Ogawa, K., 1993. Fodrin is a constituent of the cortical lattice in outer hair cells of the guinea pig cochlea: Immunocytochemical evidence. Hear. Res. 65, 274–280.

Raphael, Y., Wroblewski, R., 1986. Linkage of sub-membrane cisterns with the cytoskeleton and the plasma membrane in cochlear outer hair cells. J. Submicrosc. Cytol. Pathol. 18, 731–737.

Saito, K., 1983. Fine structure of the sensory epithelium of guinea-pig organ of Corti: Subsurface cisternae and lamellar bodies in the outer hair cells. Cell Tissue Res. 229, 467–481.

Slepecky, N., Ulfendahl, M., 1988. Glutaraldehyde induces cell shape change in isolated outer hair cells from the inner ear. J. Submicrosc. Cytol. Pathol. 20, 37–45.

Wada, H., Usukura, H., Takeuchi, S., Sugawara, M., Kakehata, S., Ikeda, K., 2001. Distribution of protein motors along the lateral wall of the outer hair cell. Hear. Res. 162, 10–18.

Wada, H., Usukura, H., Sugawara, H., Katori, Y., Kakehata, S., Ikeda, K., Kobayashi, T., 2003. Relationship between the local stiffness of the outer hair cell along cell axis and its ultrastructure observed by atomic force microscopy. Hear. Res. 177, 61–70.

Zheng, J., Shen, W., He, D.Z.Z.Z., Madison, L.D., Dallos, P., 2000. Presfin is the motor protein of cochlear outer hair cells. Nature 405, 149–155.

Zine, A., Schweitzer, L., 1997. Localization of proteins associated with the outer hair cell plasma membrane in the gerbil cochlea. Neuroscience 80, 1247–1254.

Stable Expression of the Motor Protein Prestin in Chinese Hamster Ovary Cells*

Koji IIDA**, Kazuaki KONNO**, Takeshi OSHIMA***,
Kouhei TSUMOTO****, Katsuhisa IKEDA***,
Izumi KUMAGAI****, Toshimitsu KOBAYASHI***
and Hiroshi WADA**

Mammalian hearing sensitivity relies on a mechanical amplification mechanism involving the outer hair cells (OHCs), which rapidly alter their longitudinal length in response to changes in their membrane potential. The molecular basis of this mechanism is thought to be a motor protein embedded in the lateral membrane of the OHCs. Recently, this motor protein was identified and termed prestin. Since then, prestin has been researched intensively to elucidate the behavior of the OHCs. However, little progress in the study of prestin at the molecular level has been made because no method of obtaining an adequate amount of prestin has been established. In this study, therefore, an attempt was made to construct a stable expression system of prestin using Chinese hamster ovary (CHO) cells. The expression of prestin in the transfected CHO cells and the activity of prestin on CHO cells were confirmed by immunofluorescence and whole-cell patch-clamp measurements, respectively.

Key Words: Acoustic, Biomechanics, Measurement, Outer Hair Cell, Prestin, Chinese Hamster Ovary Cell, Cloning, Patch Clamp Technique

1. Introduction

Outer hair cells (OHCs) of the mammalian cochlea are able to elongate and contract in response to changes in the membrane potential, which is known as electromotility[1]-[5]. This electromotility is believed to be the major factor in cochlear amplification that enables the high sensitivity, dynamic range and frequency selectivity of hearing in mammals (Fig. 1).

Based on whole-cell patch-pipette recording, the electromotility of the OHC has been reported to be associated with nonlinear gating charge movement or nonlinear capacitance[6]. In addition, simulation has indicated that a similar nonlinear charge movement is closely related to the conformational change of the membrane particles of the OHC[7]. According to these findings, the motility of the OHC is thought to be based on voltage-dependent conformational changes of membrane particles which are called motor proteins. It is presumed that these motor proteins are embedded in the plasma membrane of the OHC lateral wall (Fig. 2).

Recently, this motor protein was identified from gerbil cochlea and termed prestin[8]. Since its identification, prestin has been researched intensively to elucidate the characteristic behavior of the OHCs. In 2002, prestin knockout mice were constructed, and it was shown that targeted deletion of prestin in mice resulted in a loss of outer hair cell electromotility *in vitro* and a 40-60 dB loss of cochlear sensitivity *in vivo*[9].

For further study of prestin, it is necessary to research prestin at the molecular level. For this reason, a method of obtaining a large amount of

* Received 18th June, 2003 (No. 03-4090)
** Department of Bioengineering and Robotics, Tohoku University, Aoba-yama 01, Sendai 980-8579, Japan. E-mail: iida@wadalab.mech.tohoku.ac.jp
*** Department of Otolaryngology-Head and Neck Surgery, Tohoku University School of Medicine, 1-1 Seiryo-machi, Sendai 980-8575, Japan
**** Department of Biochemistry and Engineering, Tohoku University, Aoba-yama 07, Sendai 980-8579, Japan

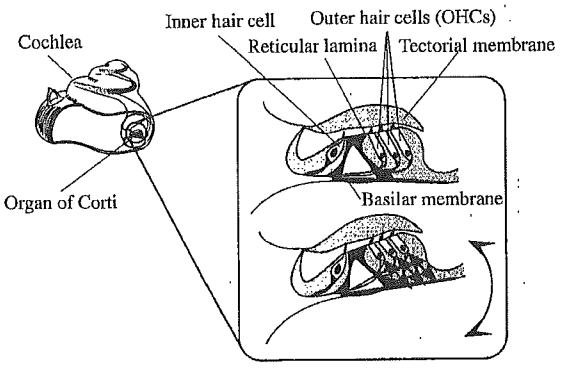

Fig. 1 Schematic of the cochlea and a cross section of the organ of Corti. When the basilar membrane undergoes an oscillatory motion, it produces a relative motion between the reticular lamina and the tectrial membrane. This motion leads to the deflection of the stereocilia of the IHC and OHCs. Ion flow into the cells and intracellular depolarization causes auditory nerve fiber activation in the IHC. Simultaneously, OHCs show a motile response and apply force to the basilar membrane of the organ of Corti. The motile response of OHCs leads to amplification of the basilar membrane. This mechanism results in the fine tuning and the wide dynamic range of the mammalian cochlea.

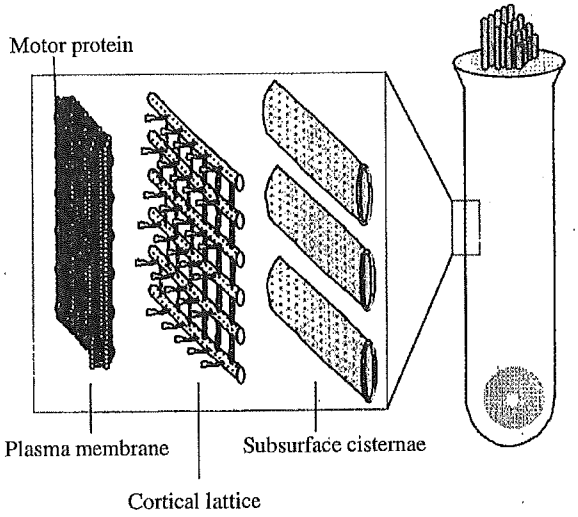

Fig. 2 Lateral wall of the OHC. The OHC lateral wall consists of three layers: plasma membrane, cortical lattice and subsurface cisternae. The motor protein is believed to be embedded in the plasma membrane.

prestin is required. However, no large-scale preparation of prestin has been reported. In this study, therefore, an attempt was made to construct the mass expression system of prestin. First, prestin cDNA was cloned from the gerbil cochlea. This cDNA was then introduced into *Escherichia coli* (*E. coli*), insect

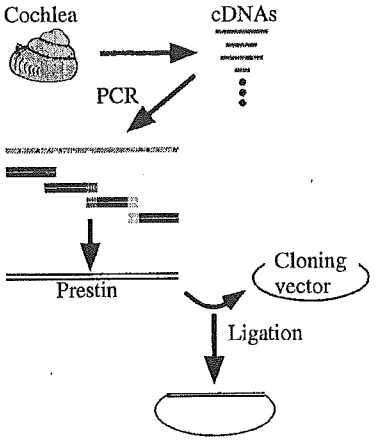

Fig. 3 Schematic representation of the cloning of prestin. The cDNAs were extracted from gerbil cochlea. From this cDNA library, four prestin fragments were obtained by PCR. These fragments were combined and inserted into cloning vector.

cells and Chinese hamster ovary (CHO) cells, and the expression of prestin was examined by Western blotting. It was verified that only CHO cells expressed prestin. Finally, limiting dilution cloning was done to generate prestin expressing cell lines using transfected CHO cells, and the expression of prestin in the generated cell line and the activity of prestin on the cell line were confirmed by immunofluorescence and whole-cell patch-clamp measurements, respectively.

2. Materials and Methods

2.1 Cloning of gerbil prestin

Prestin cDNA is necessary to express prestin in transfected cells. Therefore, a cDNA library was constructed from mRNA isolated from gerbil cochleae and prestin cDNA was cloned. A schematic representation of cloning of prestin is presented in Fig. 3. Seven adult gerbils were decapitated and their temporal bones were removed. In this study, the care and use of the animals were approved by the Institutional Animal Care and Use Committee of Tohoku University, Sendai, Japan. After the bullas were opened, the cochleae were dissected. Polyadenylated RNA was extracted from the dissected cochleae using a QuickPrep *Micro* mRNA Purification Kit (Amersham Pharmacia Biotech, Buckinghamshire, UK). Reverse transcription was performed by a First-Strand cDNA Synthesis Kit (Amersham Pharmacia Biotech).

Four fragments of prestin were amplified from this cDNA library using polymerase chain reaction (PCR) with KOD Plus (TOYOBO, Osaka, Japan). Eight primers were designed according to the gerbil prestin sequence[8]. The primers used for amplifying

the first 645 bp fragment of prestin were 5′-AAATGCTCGTCTCCTGCTGTTGGTGAAT-3′ as the forward primer and 5′-GGCCACAAATCCAAACCTGCAC-3′ as the reverse primer. For the second 613 bp fragment of prestin, 5′-GTGCAGGTTTGGATTTGTGGCC-3′ was used as the forward primer and 5′-GCGAGACAAGGAGCAGGAAATG-3′ as the reverse primer. For the third 549 bp fragment of prestin, 5′-CCTTGTCTCGCAGCCTTGTTCA-3′ was used as the forward primer and 5′-CGTACTTCCTCATGGCCTTCCT-3′ as the reverse primer. For the fourth 626 bp fragment of prestin, 5′-CATGAGGAAGTACGCAAAGGAA-3′ was used as the forward primer and 5′-ACTACTAACATTTTCCTTGGGGGTTGGG-3′ as the reverse primer. Four fragments of the prestin coding sequence were combined using a PCR-based overlap extension. The final PCR product was inserted into a pCR-Blunt II-TOPO vector (Invitrogen, Carlsbad, CA).

2.2 Plasmid construction

2.2.1 *E. coli* expression vectors When prestin cDNA is introduced into living cells using an expression vector, mRNA and protein are produced in cells. The expression vector is designed to produce a large amount of stable mRNA that will be efficiently translated into protein in transfected cells. We used pET28b (Novagen, Madison, WI), pET20b (Novagen) and pMAL-c2 (New England Biolabs, Beverly, MA) *E. coli* expression vectors. DNA was amplified by PCR from the pCR-Blunt II-TOPO vector containing prestin cDNA as a template. The *Nco*I site was added at its 5′ end and the stop codon was removed. The *Xho*I site was also added and the reading frame with the His_6-tag of the pET28b or pET20b vector was maintained at its 3′ end using primers. This DNA product was restricted with *Nco*I and *Xho*I, and ligated into the multiple cloning site of the pET28b or pET20b expression vector. In the same way, but without deletion of the stop codon, the full length of prestin was inserted into the pMAL-c2 expression vector using *Eco*RI and *Hind*III to express prestin as a maltose binding protein (MBP) fusion protein. Furthermore, cDNA fragment coding for 207, 239, 273 or 520 amino-terminal amino acids residues of prestin were similarly inserted into the pMAL-c2 expression vector with *Eco*RI and *Hind*III.

2.2.2 Baculovirus transfer vectors We used the pVL1392 baculovirus transfer vector (PharMingen, San Diego, CA). DNA was amplified by PCR from the pET28b vector containing prestin cDNA, which is described above, as a template. The *Eco*RI site was added before the start codon and the *Bam*HI site was added after His_6-tag using primers. This DNA product was inserted into the multiple cloning site of the pVL1392 baculovirus transfer vector using the *Eco*RI and *Bam*HI sites.

2.2.3 Mammalian expression vectors We used the pIRES-hrGFP-1a (Stratagene) mammalian expression vector. The pCR-Blunt II-TOPO vector containing prestin cDNA was restricted with *Not*I and *Bam*HI and ligated into the multiple cloning site of the pIRES-hrGFP-1a mammalian expression vector.

Additionally, for the immunofluorescence experiment, C-terminal FLAG-tagged prestin was constructed. DNA was amplified by PCR from the pCR-Blunt II-TOPO vector containing prestin cDNA as a template. The *Not*I site was added at its 5′ end and the stop codon was removed. The *Xho*I site was added and the reading frame with the FLAG tag of the pIRES-hrGFP-1a vector was maintained at its 3′ end using primers. This amplified DNA was inserted into the pIRES-hrGFP-1a vector.

2.3 Gene introduction, cell culture and confirmation of the expression

2.3.1 The case of *E. coli* By adding expression vectors to competent cells, which can uptake exogenous DNA, and applying a heat shock to them, expression vectors are introduced into *E. coli*. The *E. coli* strain BL21 was transformed with the pET28b or pET20b expression vector containing prestin, and the *E. coli* strain JM109 was transformed with the pMAL-c2 expression vector containing prestin. A single colony was inoculated with 3 ml Luria-Bertani (LB) medium and incubated overnight at 37°C with shaking. This overnight preculture was inoculated with 200 ml fresh LB medium and cultured. When the bacteria had grown to an optical density at 600 nm of 0.6, IPTG was added to a final concentration of 1 mM. After 2-5 h, cells were harvested and the expression of prestin in bacteria was examined by Western blotting, a method to detect specific proteins in which a complex mixture of proteins is fractionated into a series of discrete protein bands arranged in order of molecular weight on gel by SDS polyacrylamid-gel electrophoresis. A specific protein can be identified after its fractionation on gel by exposing all the proteins to a specific antibody that has been coupled to an easily detectable enzyme. When the target protein is expressed, a band is detected at its molecular weight by this procedure. When pET28b or pET20b was used, expression was examined by anti-His_6 antibody (Invitrogen), and when pMAL-c2 was used, expression was examined by anti-MBP antibody (New England Biolabs).

2.3.2 The case of insect cells To introduce an exotic gene into insect cells, a recombinant baculovirus was applied to them. One microgram of BaculoGold linearized DNA (PharMingen) and prestin trans-

fer vector were co-transfected into Sf9 cells cultured in IS BAC medium (Irvine Scientific, Santa Ana, CA) using Lipofection Reagent (Invitrogen). The cells were incubated for 3 days. Virions released in the medium were amplified to a virus titer of 1×10^7 pfu/ml. Sf9 cells were plated onto a 35-mm plate with 2 ml of fresh medium and inoculated with 200 μl of recombinant baculovirus. After incubation for 3 days, cells were harvested and expression of prestin in Sf9 cells was examined by Western blotting using anti-His_6 antibody.

2.3.3 The case of CHO cells To introduce expression vectors into CHO cells by endocytosis, a mixture of an expression vector and a lipid is added to CHO cells according to the following procedure. The CHO cells (provided by the Cell Resource Center for Biomedical Research, Tohoku University) were cultured in RPMI-1640 medium with 10% fetal bovine serum, 100 U penicillin/ml and 100 mg streptomycin/ml at 37°C with 5% CO_2. The CHO cells were plated onto a 35-mm culture dish for 24 h before transfection. Two hundred and fifty microliters of D-MEM was combined with 15 μl of 1 mg/ml LipofectAMIN 2000 (Invitrogen) and incubated at room temperature for 4 min. Two hundred and fifty microliters of D-MEM was also combined with 4 - 5 μg of expression vector containing FLAG-tagged prestin cDNA. These two solutions were then combined and complexed for 20 min at room temperature. After 20 min of complexing, the culture medium was replaced with 2 ml of fresh medium without antibiotic and 500 μl of D-MEM/DNA/LipofectAMINE 2000 mixture was added to the culture. After 24 h of transfection, the medium was replaced with fresh RPMI-1640 medium containing FBS and antibiotic. After incubation for 2 days at 37°C with 5% CO_2, cells were harvested and expression of prestin in CHO cells was examined by Western blotting using anti-FLAG antibody (Sigma-Aldrich, St. Louis, MO).

2.4 Generation of prestin expressing CHO cell lines

It was confirmed that only CHO cells expressed prestin. Therefore, an attempt was made to generate the prestin expressing cell lines using transfected CHO cells. Prestin cDNA or FLAG-tagged Prestin cDNA were transfected into CHO cells as described above. After 24 h of transfection, cells were diluted to 5 cells/ml in fresh RPMI-1640 medium with FBS and antibiotic and then plated out at 200 μl/well in 96-well tissue culture plates. Plates were incubated at 37°C with 5% CO_2 for 14 days. Single colonies contained in 96-well plates were scaled up to 24-well plates. After 5 days of culturing, transfected clones were chosen based on the fluorescence of green fluorescent protein (GFP) using a fluorescent microscope, because the pIRES-hrGFP-1a vector includes the GFP gene. The clones, in which the expression of GFP was confirmed, were cultured in T-25 flasks.

2.5 Immunofluorescence experiments

CHO cells transfected with FLAG tagged prestin and untransfected CHO cells were fixed with 10% formalin in phosphate buffer for 5 min at room temperature and washed with PBS buffer. The samples were then incubated with skim milk and fetal bovine serum. After PBS washing, cells were incubated with anti-FLAG primary antibody (Sigma-Aldrich) in PBS with 0.1% saponin solution for 1 h at 37°C. The samples were then washed with PBS and incubated with TRITC-conjugated anti-mouse IgG secondary antibody (Sigma-Aldrich) in PBS with 0.1% saponin solution for 30 min at 37°C. Finally, the samples were washed with PBS, and immunofluorescence images of the all samples were obtained using a confocal laser scanning microscope (LSM-GB200, Olympus, Tokyo, Japan).

2.6 Electrophysiological measurements

A pipette for whole-cell patch-clamp recordings was formed on a programmable puller (PP-830, Narishige) from a glass tube. The pipette resistance was typically 2-3 MΩ when measured in a bath. It was filled with a solution composed of 140 mM KCl, 3.5 mM $MgCl_2$, 5 mM EGTA, 5 mM HEPES, 0.1 mM $CaCl_2$ and 2.5 mM Na_2ATP, adjusted to pH 7.3. The bath solution contained 145 mM NaCl, 5.8 mM KCl, 1.3 mM $CaCl_2$, 0.9 mM $MgCl_2$, 10 mM HEPES, 0.7 mM Na_2HPO_4 and 5.6 mM glucose, adjusted to pH 7.3.

A block diagram of the measurement system is shown in Fig. 4. This system consists of a patch amplifier (Axopatch 200B amplifier, Axon Instruments, Foster City, CA), an A/DD/A converter (Digidata 1320A, Axon Instruments), a personal computer and a function generator (WF1944, NF Electronic Instruments, Kanagawa, Japan). Measurements of cell capacitance were performed using the "membrane test" feature of pCLAMP 8.0 acquisition software (Axon Instruments). A test square wave (amplitude, 20 mV ; period T=4 msec, i.e., frequency, 250 Hz) was generated by the personal computer controlled by pCLAMP 8.0 software and applied to the cell through the amplifier. The transient current, which is caused by the test square wave, was then sampled through the amplifier. The patch-clamp parameters, i.e., membrane capacitance, membrane resistance, access resistance, the time constant of the current decay and the steady state holding current, were continuously calculated by pCLAMP 8.0 software from this current (see Appendix). Each calculated parameter, which was obtained from 10 positive

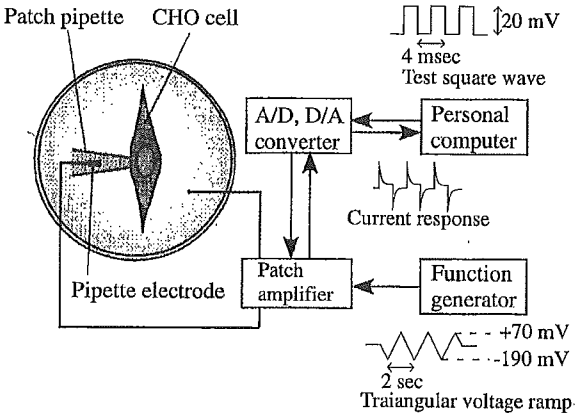

Fig. 4 Block diagram of the measurement system. This system consists of a patch amplifier, an A/DD/A converter, a personal computer and a function generator. Test square waves and triangular voltage ramps were generated by the personal computer and function generator, respectively. These waves were superimposed and applied to the cell through the amplifier. The transitional current was then measured and the membrane capacitance was calculated from this current.

and 10 negative consecutive test steps, was averaged and saved to the personal computer every 40 msec, i.e., a time resolution of 25 Hz, and these parameters were monitored through measurements in real time.

To determine the voltage dependence of membrane capacitance, triangular voltage ramps were superimposed on the test square wave mentioned above. This triangular voltage wave (period $T=2$ sec) was generated by a function generator and swung the cell potential from -190 mV to $+70$ mV. The ramps were applied to the cell for 6 sec (3 cycles)[10]. The data measured in the first ramp were analyzed because the cells were damaged by reiteration of voltage stimulations.

After the measurements, the values of membrane capacitance, which were obtained when the membrane potential of the cell was ramped from -140 mV to $+70$ mV, were plotted versus membrane potential. The membrane capacitance was fitted to the derivative of a Boltzmann function[6],

$$C_m = C_{lin} + \frac{Q_{max}}{\alpha e^{\frac{V-V_{1/2}}{\alpha}}\left(1+e^{-\frac{V-V_{1/2}}{\alpha}}\right)^2} \quad (1)$$

where C_{lin} is linear capacitance, Q_{max} is maximum charge transfer, V is membrane potential and $V_{1/2}$ is the voltage at which the maximum charge is equally distributed across the membrane. In Eq. (1), α is the slope factor of the voltage dependence of the charge transfer and is given by

$$\alpha = kT/ze, \quad (2)$$

where k is Boltzmann's constant, T is absolute temperature, z is valence and e is electron charge.

3. Results

3.1 Examination of the expression of prestin by Western blotting

cDNA encoding the full length of prestin was obtained by PCR. This cDNA was introduced into *E. coli*, insect cells and CHO cells. The full length of prestin was not expressed in *E. coli* using any expression vector. Only the 207 amino-terminal amino acids of prestin which fused with MBP were expressed in *E. coli* using the pMAL-c2 vector. When cDNA encoding longer prestin fragments was introduced into *E. coli*, it was not expressed at all. When the baculovirus expression system was used, the full-length of prestin was expressed in Sf9 cells. However, the expression level was very low and expressed prestin was fragmented. By contrast, the full-length of prestin was expressed in CHO cells. Therefore, an attempt was made to construct cell lines which express prestin.

3.2 Generation of CHO cell lines which express prestin

In the case of FLAG-tagged prestin, after transfection, CHO cells were plated out into 96 wells. Twenty-one wells contained a single colony and the growth of 13 of them was good. The expression of the GFP was confirmed in these 13 clones, two of which were found to express GFP. These cell lines were used for immunofluorescence experiments.

In the case of CHO cells expressing prestin without a tag, cells were plated out into 96 wells. Twenty-six wells contained a single colony and the growth of 22 of them was good. The expression of the GFP was confirmed in these 22 clones and two of them were found to express GFP. One of the generated clones was analyzed by electrophysiological measurement.

3.3 Immunofluorescence experiments

As shown in Fig. 5, the plasma membrane of a generated cell line expressing FLAG-tagged prestin was stained by immunofluorescence. Staining was observed in almost all cells. By contrast, untransfected cells were not stained. These results show that tagged prestin is expressed in the plasma membrane of CHO cells.

3.4 Electrophysiological measurements

First, the electrophysiological properties of the plasma membrane of OHCs were measured. The membrane capacitance versus membrane potential measured in one OHC is shown in Fig. 6. These values were measured when the first voltage ramp was applied to the OHC. It exhibited bell-shaped nonlinear membrane capacitance in response to ramping of the transmembrane voltage. This nonlinear mem-

(a)

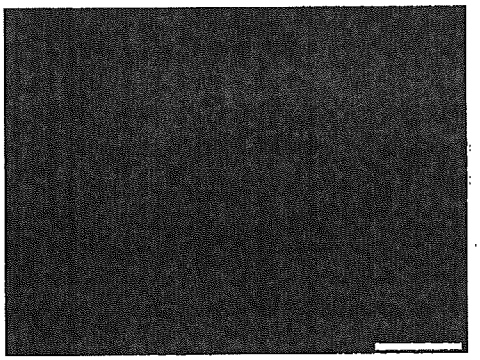

(b)

Fig. 5 Immunofluorescence image of CHO cells transfected with FLAG-tagged prestin and that of normal CHO cells. (a) FLAG-tagged prestin transfected CHO cells. (b) Untransfected CHO cells. Fluorescent stains were observed in transfected cells. By contrast, untransfected cells were not stained. These results indicate that FLAG-tagged prestin was expressed in the plasma membrane of transfected CHO cells. Scale bars are 50 μm.

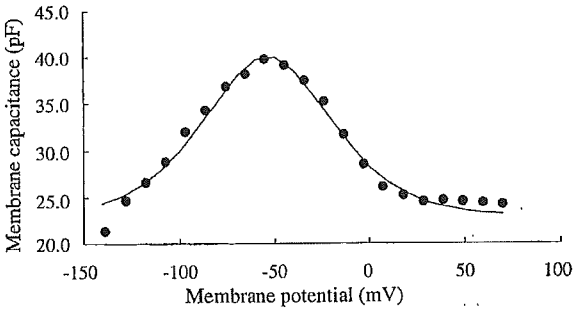

Fig. 6 Representative data of voltage dependence charge movement of four independent OHCs. Voltage was ramped from −190 to 70 mV. The filled circles show the measured membrane capacitance of the first ramp from −140 mV to +70 mV versus membrane potential. Data points displayed by filled circles were fitted with the derivative of a Boltzmann function (Eq. (1)), which is shown by the solid line, with the following parameters: C_{lin} =22.8 pF, Q_{max}=1.59 pC, α=22.9 mV and $V_{1/2}$= −53.8 mV.

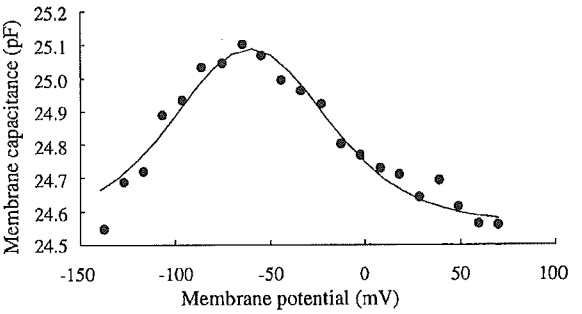

(a)

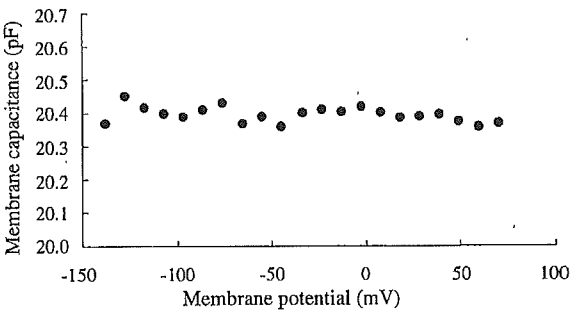

(b)

Fig. 7 Representative data of voltage dependence charge movement of nine independent CHO cells expressing prestin and nine independent untransfected CHO cells. The filled circles show the measured membrane capacitance of the first ramp from −140 mV to +70 mV versus membrane potential. (a) Membrane capacitance of a CHO cell expressing prestin. Data points displayed by filled circles were fitted with the derivative of a Boltzmann function (Eq. (1)), which is shown by the solid line, with the following parameters: C_{lin}=24.6 pF, Q_{max}=57.0 fC, α=27.0 mV and $V_{1/2}$=−60.6 mV. (b) Membrane capacitance of a normal CHO cell.

brane capacitance was well fitted with a derivative of a Boltzmann function (Eq. (1)). Four cells were measured and the values of membrane capacitance were fitted with Eq. (1). The fit parameters of Eq. (1) were obtained as C_{lin}=20.1±2.4 pF, Q_{max}=2.17 ±0.60 pC, α=26.2±4.1 mV and $V_{1/2}$=−43.4±10.4 mV (n=4, mean±SD). These values correspond fairly well with those previously reported[11].

The voltage-dependent charge movement of the generated cell line expressing prestin was then measured. As shown in Fig. 7(a), prestin-expressed cells exhibited bell-shaped nonlinear membrane capacitance in response to ramping of transmembrane voltage. This nonlinear membrane capacitance was well fitted with Eq. (1) that describes the nonlinear membrane capacitance observed in OHCs. In a group of 9 cells, these curve fits yielded values of C_{lin}=19.8±3.2 pF, Q_{max}=59.7±33.7 fC, α=32.9±5.9 mV and $V_{1/2}$=

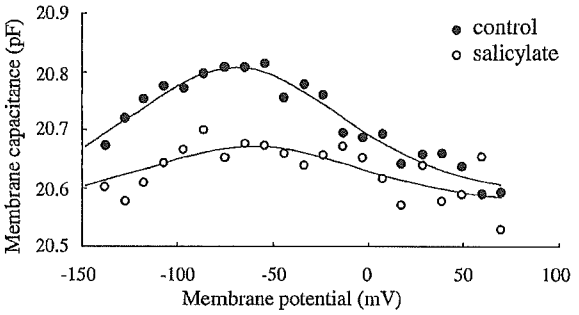

Fig. 8 Effect of localized application of 10 mM sodium salicylate on the charge movement of a CHO cell expressing prestin. The measured membrane capacitance of the first ramp from −140 mV to +70 mV is plotted versus membrane potential. The filled circles show the membrane capacitance versus membrane potential before salicylate treatment and the open circles show this potential after salicylate treatment. Data points displayed by filled circles and open circles were fitted with the derivative of a Boltzmann function (Eq. (1)), which is shown by the solid line, with the following parameters: C_{lin}=20.6 pF, Q_{max}=34.7 fC, α=38.6 mV and $V_{1/2}$=−69.5 mV (control); and C_{lin}=20.6 pF, Q_{max}=15.6 fC, α=38.8 mV and $V_{1/2}$=−60.4 mV (salicylate), respectively.

−60.6±11.0 mV (mean±SD). By contrast, untransfected cells (n=9) had no measurable nonlinear membrane capacitance (Fig. 7(b)). These values are quite similar to those obtained from CHO cells transiently expressing prestin[12].

It is known that nonlinear membrane capacitance is blocked by sodium salicylate in OHCs[13]. To confirm that nonlinear membrane capacitance was caused by prestin, sodium salicylate was applied to the cells. A puff pipette was filled with 10 mM sodium salicylate dissolved in extracellular solution, and salicylate was locally applied to a cell that had been shown to have nonlinear membrane capacitance. Sodium salicylate reduced nonlinear membrane capacitance (n=1, Fig. 8).

4. Discussion

To obtain a large amount of prestin, we attempted to construct of the expression system of prestin using *E. coli* and baculovirus. However, these approaches eventuated in failure. By contrast, prestin was found to be stably expressed in a mammalian cell line. It is presumed that because the constitution of the membrane of *E. coli* is quite different from the mammalian plasma membrane, membrane protein prestin was not expressed in *E. coli*. In addition, because insect cells and prestin derived mammalian OHCs may be incompatible, the expression level is very low in insect cells. By contrast, prestin was more easily expressed in mammalian cells. In this study, we were indeed able to generate cell lines expressing prestin using CHO cells.

The plasma membrane of the cells expressing FLAG-tagged prestin was stained by immunofluorescence. These results indicate that prestin is expressed in the plasma membrane of the cell and are in agreement with the presumption that prestin exists in the plasma membrane of OHCs[14].

The results of electrophysiological measurements showed that the prestin expressed in CHO cells was active. The expression level of prestin in the generated cell line was then estimated using the obtained linear capacitance, C_{lin}, and the maximum charge transfer, Q_{max}. The method of obtaining the charge density of the cell, the charge movement of which is shown in Fig. 7(a), is as follows. As C_{lin} indicates the total capacitance of the plasma membrane of the cells, and the membrane capacitance of the cells per unit area is known to be 0.01 pF/μm²[15], the surface area was found to be 2,460 μm² (24.6/0.01) when C_{lin} was 24.6 pF. The charge density, i.e., Q_{max} divided by the surface area, was then determined to be 144 $e^-/\mu m^2$ ($57.0\times10^{-15}/(1.60\times10^{-19}\times2\,460)$), when Q_{max} was 57.0 fC and e^- is 1.60×10^{-19} C. In this way, the averaged charge density of the 9 measured cells was obtained to be 196 $e^-/\mu m^2$. Although this value is lower than those of OHCs (7 500 $e^-/\mu m^2$)[11] and TSA201 cells transiently expressing prestin (5 360 $e^-/\mu m^2$)[8], the stable expression of prestin in the generated cell line is an advantage of this study.

5. Conclusions

Prestin cDNA was cloned from gerbil cochlea. Prestin was found to be expressed in mammalian cells, but not in *E. coli* and insect cells. A prestin expressing cell line was generated with CHO cells by limiting dilution cloning. The expression and activity of prestin in the generated cell lines were confirmed by immunofluorescence and whole-cell patch-clamp measurements, respectively. Although the expression level was lower than those of OHCs and TSA201 cells which transiently express prestin, the generated cell line was confirmed to stably express active prestin. A stable expression system of prestin was thus constructed.

Acknowledgments

This work was supported by a grant from the Human Frontier Science Program, by a Health and Labour Science Research Grant from the Ministry of Health, Labour and Welfare of Japan, and by Grant-in-Aid for Scientific Research on Priority Areas

15086202 from Ministry of Education, Culture, Sports, Science and Technology of Japan.

Appendix

The equivalent circuit of the cell with a whole-cell patch-clamp is shown in Fig. 9(a), where R_a is the electrode access resistance, R_m is the membrane resistance and C_m is the membrane capacitance. The current in response to a square voltage wave is displayed in Fig. 9(b). For this model, the steady state current I_{ss} and the instantaneous current I_0 are expressed by

$$I_{ss}=V_\Delta/(R_a+R_m), \tag{3}$$

$$I_0=V_\Delta/R_a, \tag{4}$$

when a voltage step V_Δ is applied to the circuit. The exponentially decaying current $I(t)$ is given by

$$I(t)=(I_0-I_{ss})\exp(-t/\tau)+I_{ss}. \tag{5}$$

In Eq. (5), t is the time, and τ is the time constant given by

$$\tau=R_pC_m, \tag{6}$$

where

$$R_p=\frac{R_aR_m}{R_a+R_m}. \tag{7}$$

The total resistance R_t is defined as

$$R_t=R_m+R_a. \tag{8}$$

The unknown values, i.e., membrane capacitance C_m, access resistance R_a and membrane resistance R_m, are determined as follows using the measured current. The membrane capacitance C_m is given by

$$C_m=(Q_1+Q_2)/V_\Delta, \tag{9}$$

where Q_1 is the charge in the transient above the steady-state response and Q_2 is the correction factor as shown in Fig. 9(b). They are expressed by

$$Q_1=\int(I(t)-I_{ss})dt, \tag{10}$$

$$Q_2=I_{ss}\tau. \tag{11}$$

The time constant τ is obtained by a logarithmic fit. By substituting Q_1 and Q_2 obtained from Eqs. (10) and (11) into Eq. (9), the membrane capacitance C_m is acquired.

The access resistance R_a is determined as follows. The total resistance R_t is given by

$$R_t=V_\Delta/I_{ss}, \tag{12}$$

and this is obtained from the steady-state response. From Eqs. (6), (7) and (8), the equation is drawn in the form

$$R_a^2-R_aR_t+R_t(\tau/C_m)=0. \tag{13}$$

Substituting the obtained values of R_t, τ and C_m into Eq. (13) and using the Newton-Raphson method, R_a is acquired. Finally, the membrane resistance R_m is acquired by substituting the obtained values of R_t and R_a into Eq. (8).

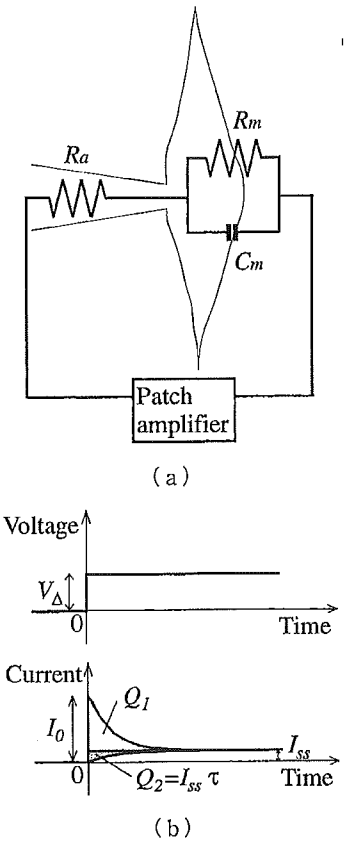

Fig. 9 Measurement of the membrane capacitance. (a) Scheme of an idealized circuit representing the capacitive cell response. C_m, membrane capacitance; R_a, pipette access resistance; R_m, cell membrane resistance. (b) A step-change in membrane voltage (top) elicits a transient membrane current (bottom). From this current, the total charges that are translocated across the membrane are calculated. I_0 is the peak response, I_{ss} is the steady-state current, τ is the time constant, Q_1 is the charge in the transient above the steady-state response and Q_2 (dashed area) is the correction factor.

References

(1) Brownell, W.E., Bader, D. and Ribaupierre, Y., Evoked Mechanical Responses of Isolated Cochlear Outer Hair Cells, Science, Vol. 227 (1985), pp. 194-196.

(2) Kachar, B., Brownell, W.E., Altschuler, R. and Fex, J., Electrokinetic Shape Changes of Cochlear Outer Hair Cells, Nature, Vol. 322 (1986), pp. 365-368.

(3) Zenner, H.P., Motile Responses in Outer Hair Cells, Hear. Res., Vol. 22 (1986), pp. 83-90.

(4) Ashmore, J.F., A Fast Motile Response in Guinea-Pig Outer Hair Cells: The Cellular Basis of the Cochlear Amplifier, J. Physiol., Vol. 388 (1987), pp. 323-347.

(5) Santos-Sacchi, J. and Dilger, J.P., Whole Cell Currents and Mechanical Responses of Isolated Outer Hair Cells, Hear. Res., Vol. 35 (1988), pp.